Available online at www.sciencedirect.com
ScienceDirect
Trans. Nonferrous Met. Soc. China 24(2014) 712−717
Transactions of Nonferrous Metals Society of China
www.tnmsc.cn

$Fe_{75}Zr_3Si_{13}B_9$ magnetic materials prepared by spark plasma sintering

Xing-hua WANG[1], Ge WANG[1], Yu-ying ZHU[1], Jin-feng BAO[1], Xiong-fei DU[1], Qiang LI[1,2,3]

1. National Engineering Research Center for Equipment and Technology of Cold Strip Rolling, Yanshan University, Qinhuangdao 066004, China;
2. National Key Laboratory of Metastable Materials Science and Technology, Yanshan University, Qinhuangdao 066004, China;
3. College of Materials Science and Engineering, Hebei University of Technology, Tianjin 300401, China

Received 17 April 2013; accepted 5 July 2013

Abstract: $Fe_{75}Zr_3Si_{13}B_9$ magnetic amorphous powders were fabricated by mechanical alloying. Bulk amorphous and nanocrystalline alloys with 20 mm in diameter and 7 mm in height were fabricated by the spark plasma sintering technology at different sintering temperatures. The phase composition, glass transition temperature (T_g), onset crystallization temperature (T_x), peak temperature (T_p) and super-cooled liquid region (ΔT_x) of $Fe_{75}Zr_3Si_{13}B_9$ amorphous powders were analyzed by X-ray diffraction (XRD) and differential scanning calorimetry (DSC). The phase transition, microstructure, mechanical properties and magnetic performance of the bulk alloys were discussed with X-ray diffractometer, scanning electron microscope (SEM), Gleeble 3500 and vibration sample magnetometer (VSM), respectively. It is found that with the increase in the sintering temperature at the pressure of 500 MPa, the density, compressive strength, micro-hardness and saturation magnetization of the sintering samples improved significantly, the amorphous phase began to crystallize gradually. Finally, the desirable amorphous and nanocrystalline magnetic materials at the sintering temperature of 863.15 K and the pressure of 500 MPa have a density of 6.9325 g/cm^3, a compressive strength of 1140.28 MPa and a saturation magnetization of 1.28 T.

Key words: mechanical alloying; amorphous and nanocrystalline alloys; saturation magnetization; spark plasma sintering

1 Introduction

Spark plasma sintering (SPS) technology developed in the 1990s is a energy-conservation, environmental protection and novel highly-efficient technology for preparing materials, which combines plasma activation, hot pressing and resistance heating, as known as the plasma activated sintering or pulse current hot pressing sintering [1−3]. Because of rapid sintering speed, low sintering temperature, special sintering mechanism, simple and convenient operation, without powder preformed etc, SPS has been recognized as the most competitive and promising technique to successfully consolidate bulk nano-materials with high density, nanocrystalline and clean interface, and widely used for preparation or research of ceramics, intermetallics, functional gradient materials and composites [4−6]. The large DC pulsed sintering current is applied through the electrodes at the top and bottom punches of the die and also flowed through the compacted powders. The Joule heat is generated instantaneously between the surfaces of particles, which produces local high temperature and achieves formation and diffusion of the sintering neck. Meanwhile, the pulse current causes discharge effect among particles, which can purify the surface of particles, restrict the growth of grain and realize the densification under high pressure [7,8].

Since the ‘Finemet’ alloys were fabricated in amorphous matrix through heat treatment by YOSHIZAWA et al [9], Fe-based nanocrystalline soft magnetic materials with excellent soft magnetic and mechanical properties have become a hot research, such as fabrication of ‘Nanoperm’ alloys in 1990 [10], ‘Hitperm’ alloys in 1998 [11], iron core materials for transformer with super lower iron loss in Japan in 2000 [12], and bulk ‘Liqualloy’ high performance soft magnetic sheet alloy in Japanese Alps Electrics Co., Ltd.

Foundation item: Project (13961001D) supported by the Key Basic Research Project of Hebei Province, China; Project (2013BAE08B01) supported by the National Key Technology R&D Program of China
Corresponding author: Qiang LI; Tel: +86-335-8063946; E-mail: liqiang@ysu.edu.cn
DOI: 10.1016/S1003-6326(14)63115-0

in 2011 [13]. However, the shapes of the above alloys prepared by rapid quenching techniques were primary ribbon and sheet so that they could not satisfy the demand for complicated shape in industrial application. So development of Fe-based bulk nanocrystalline composites by simple process, low cost, complicated shape and superior soft magnetic properties has a broad application prospect.

In this work, bulk amorphous and nanocrystalline $Fe_{75}Zr_3Si_{13}B_9$ composites were fabricated by mechanical alloying and spark plasma sintering. The sintering characteristics and the influence of sintering temperature on microstructure, mechanical properties and magnetism were investigated.

2 Experimental

Pure elemental powders of Fe (purity≥99.5%, 5−8 μm), Zr (purity≥99.9%, 38 μm), Si (purity≥99.99%, 48 μm) and B (purity≥99.99%, 48 μm) were mixed to the desired nominal composition of $Fe_{75}Zr_3Si_{13}B_9$, in stainless steel vessels with stainless steel balls, and the ball to powder mass ratio was 30:1. In order to avoid the oxidation of the mixed powders, the vessels were extracted and filled with high purity Ar gas (99.99%). Mechanical alloying was performed by a high-energy planetary ball mill (QM-3SP4) at a rotational speed of 450 r/min. The milling process was periodically interrupted every 0.5 h and each interruption was lasted 0.25 h to cool down the vessels. The as-milled powders were weighed 10 g and put into the WC hard metal mold, which had two WC hard metal punches with diameter of 20 mm. Then the powders were sintered with SPS equipment (SPS-3.20MK-IV) under a pressure of 500 MPa, at a heating rate of 30 K/min, with holding time of 10 min. The bulk amorphous and nanocrystalline $Fe_{75}Zr_3Si_{13}B_9$ magnetic alloys with a diameter of 20 mm and height of 7 mm were fabricated at different sintering temperatures, which were measured by the thermocouple.

The structures of the as-milled powders and the sintered samples were examined by X-ray diffractometry (XRD) equipment of type D/max−2500 with Cu K_α radiation. Thermal behaviors of the as-milled powders were measured with a differential scanning calorimeter (DSC, NETZSCH STA449C) at a heating rate of 30 K/min under flowing Ar gas (99.99%), and the different sintering temperatures (T_s) were selected based on the DSC results. The microstructures of the samples sintered at different temperatures were observed with scanning electron microscope (SEM, HITACHI S−4800). The density was measured by Archimedes drainage method. The compressive strength was examined with a Gleeble−3500. The microhardness was tested with a microhardness tester (FM-ARS−9000) at a load of 2.94 N with 10 s dwell time. Magnetic properties including saturation magnetization (B_s) and coercive force (H_c) were measured with vibrating sample magnetometer (VSM, Lakeshore 7404) in a maximum applied magnetic field of 800 kA/m at room temperature.

3 Results and discussion

Figure 1 shows the XRD patterns of the $Fe_{75}Zr_3Si_{13}B_9$ alloy powders by MA with different milling time. The patterns show gradually broad peak with the milling time prolonging, which indicate a typical amorphous halo peak. The diffraction peak disappeared after milling for 20 h at the 2θ angle between 64° and 67°, indicating the formation of amorphous. After milling for 30 h, the halo peaks of amorphous alloy powder were remarkable and no distinct crystalline peaks could be seen in the XRD patterns, suggesting that the alloy powders are fully amorphous. With the increase of milling time, the sharp diffraction peaks of crystal phases were observed at the 2θ angle of about 45°, indicating that increasing the milling time has disadvantage for the $Fe_{75}Zr_3Si_{13}B_9$ alloy powders to form amorphous ones. The best milling time is 30 h in the present ball-milling process.

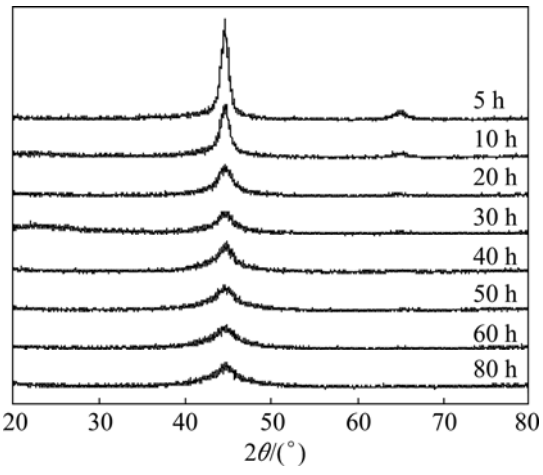

Fig. 1 XRD patterns of $Fe_{75}Zr_3Si_{13}B_9$ alloy powders with different milling time

Thermal behavior of alloy powders milled for 30 h is shown in Fig. 2. The amorphous alloy powders have remarkable exothermic peak of crystallization. The glass transition temperature T_g is 753.37 K, the onset crystallization temperature T_x is 823.61 K, the peak temperature T_p is 833.62 K, and the super-cooled liquid

region ($\Delta T_x=T_x-T_g$) is about 70.24 K. This indicates that the amorphous $Fe_{75}Zr_3Si_{13}B_9$ alloy powders exhibit good thermal stability before crystallization. Based on the characteristic temperatures of the amorphous powders, six different sintering temperatures (T_{s1}=723.15 K, T_{s2}=753.15 K, T_{s3}=793.15 K, T_{s4}=823.15 K, T_{s5}=843.15 K and T_{s6}=863.15 K) were chosen to prepare bulk samples. The T_s values were divided into the following relationship: $T_{s1}<T_{s2}\approx T_g<T_{s3}<T_{s4}\approx T_x<T_p<T_{s5}<T_{s6}$.

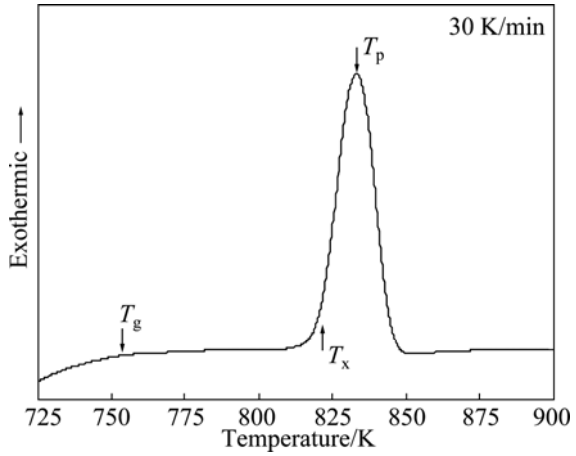

Fig. 2 DSC curve of amorphous $Fe_{75}Zr_3Si_{13}B_9$ alloy powders

Figure 3 shows the XRD patterns of the glassy powders milled for 30 h and the bulk alloys sintered at different temperatures. With the increase of the sintering temperature, XRD patterns of the bulk alloys gradually became sharp, and the crystal phases of Fe_3Si and Fe_2B emerged in amorphous matrix. As the samples were sintered below T_g, at T_{s1} and T_{s2}, the main phase still kept amorphous, but a little Fe_3Si crystal phase emerged at the 2θ angle between 65° and 67°, illustrating that the actual T_s is higher than the temperature measured by the thermal couple, which is due to a certain thickness of the inner mold between the sintered powders and the thermal couple. The heat flowing through the inner mold had a certain loss and a time lag existed. As the T_s was higher than T_{s3}, Fe_2B compound phase separated out at the 2θ angle of about 56°, and with the T_s rose to T_{s6}, the diffraction peak of the sintered samples became gradually sharp but still kept a certain amorphous halo peak, indicating that a mass of nanocrystalline phases generate in the amorphous matrix, but the addition of element Zr hinders the growth of the nanocrystalline grains and the continuous crystallization of the amorphous phase. Although the samples are sintered at higher temperature T_{s6}, they still keep amorphous and nanocrystalline structure, and amorphous and nanocrystalline composites form.

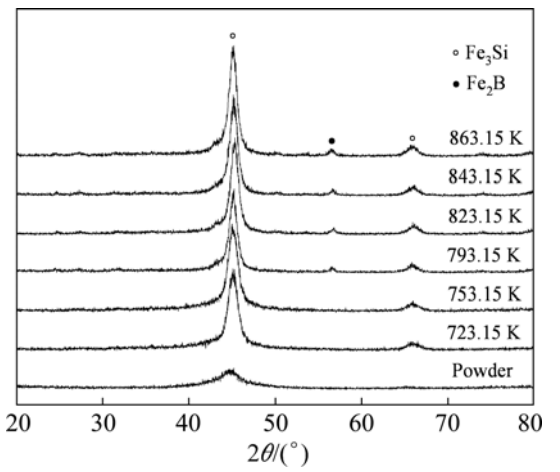

Fig. 3 XRD patterns of bulk $Fe_{75}Zr_3Si_{13}B_9$ alloys prepared by SPS at different sintering temperatures

Figure 4 shows the change of the density with the sintering temperature. The density increased from 5.6705 g/cm^3 at T_{s1} to 6.9325 g/cm^3 at T_{s6}, and reached 95.43% of the theoretical density. When the sintering temperature T_s rose from T_{s1} to T_{s6}, the density increased apparently, as a result of the remarkable viscous flow and atomic diffusion of the amorphous powders. Meanwhile, the precipitation of the nanocrystallines Fe_3Si and Fe_2B in the amorphous matrix could also enhance the density. As the T_s rose to T_{s5}, the increase of the density became slowly, indicating that the nanocrystalline phases had the priority to be amorphous in the alloy and the nanocrystalline grain tends to grow up with the increase of the T_s.

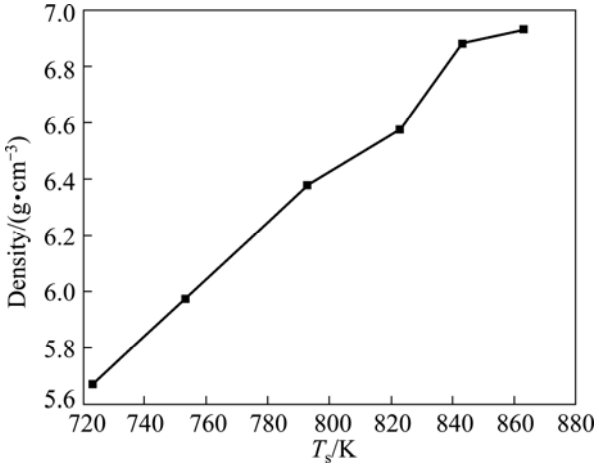

Fig. 4 Density of $Fe_{75}Zr_3Si_{13}B_9$ bulk alloys sintered by SPS at different sintering temperatures

Figure 5 shows the micro-hardness and compressive strength of the sintered samples. The hardness and the strength of the samples increased remarkably with the increase of T_s. The partial nanocrystalline phase formed in amorphous matrix, and the dispersion strengthening effect of the amorphous and nanocrystalline enhanced the hardness and strength. Meanwhile, the powders were

seamed under the effect of higher pressure and higher frequency pulse plasma current, which improve the density. The microhardness and strength at T_{s6} are HV905.32 and 1140.28 MPa, respectively.

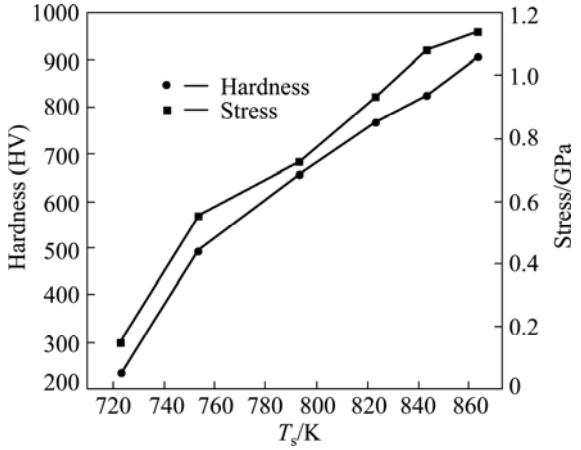

Fig. 5 Hardness and stress of $Fe_{75}Zr_3Si_{13}B_9$ bulk alloys at different sintering temperatures

Figure 6 shows the variation of the B_s and H_c. With the increase of T_s, it can be obviously observed that the B_s and H_c increased respectively from 1.01 to 1.28 T and 1.96×10^3 to 4.08×10^3 A/m. The increase of the B_s is due to the gradual increase of the density and the decrease of the free volume and resident porosities. Meanwhile, the addition of Zr effectively suppressed the growth of the solid nanocrystalline α-Fe(Si). The formation of double-phase structure of the amorphous and nanocrystalline can enhance the ferromagnetic exchange effect. When the T_s rose to T_{s5}, the B_s decreased slightly owing to the decrease of the amorphous phases and the increase of the crystalline phases Fe_2Si and Fe_3B, which weakens the ferromagnetic exchange effect. It is well known that the H_c is sensitive to the phase structure, grain size and internal microstrain of the samples. With the increase of the T_s, the nanocrystalline dissolved out

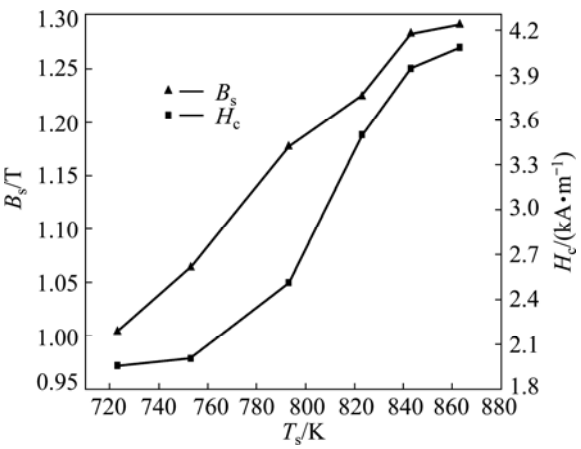

Fig. 6 B_s and H_c of $Fe_{75}Zr_3Si_{13}B_9$ bulk alloys at different sintering temperatures

from the amorphous matrix. Meanwhile, the grain boundary hindered the rotation of the magnetic domain and the movement of the magnetic domain walls, so the H_c increased with the T_s. Meanwhile, according to the nanocrystalline random anisotropic model of HERZER [14−16], for grain size D and coercive force H_c, a single magnetic domain critical size (L_{ex}) exists. If the D is smaller than the L_{ex}, the H_c is directly proportional to the D^6; if the D is greater than the L_{ex}, the H_c is inversely proportional to the D^6. Because the grain size of the nanocrystalline formed in amorphous matrix is far less than L_{ex}, and the H_c shows the tendency to increase.

The morphologies of the sintered samples at different sintering temperatures are shown in Fig. 7. The micrographs further confirmed that the density became gradually high with the increase of sintering temperature. The result is identical with Figs. 4 and 5. If T_s was lower than T_g, the samples have obvious gaps or spaces between the powder particles (Figs. 7(a) and (b)) and have lower strength and hardness. When T_s was higher than T_g and lower than T_x, because the amorphous powders have bigger viscous flow and super plasticity properties in the super-cooled liquid region, the density was improved (Figs. 7(c) and (d)). With further increasing T_s to 863.15 K, densified sample with very few pores was fabricated (Fig. 7(f)). This indicates that during the process of the amorphous powders sintered by the plasma current, the surface is alternately sintered and welded.

4 Conclusions

1) The amorphous $Fe_{75}Zr_3Si_{13}B_9$ alloy powders were successfully fabricated by mechanical alloying for 30 h with strong amorphous formation ability. The super-cooled liquid region ΔT_x is about 70.23 K.

2) The bulk amorphous and nanocrystalline $Fe_{75}Zr_3Si_{13}B_9$ alloys were synthesized by the spark plasma sintering (SPS) technology under the pressure of 500 MPa with holding time of 10 min. The compressive strength is 1140.28 MPa, microhardness is HV905.32, relative density is 95.32% and the saturation magnetization is 1.28 T.

3) With the increase of the sintering temperature T_s, the density, stress and B_s are significantly improved. The addition of Zr can suppress the growth of the nanocrystalline grains and efficiently promote the alloy forming composite structure of amorphous and nanocrystalline.

4) The α-Fe(Si) solid solution particles diffused in amorphous matrix can obviously enhance the ferromagnetic exchange coupling effect, which not only promote the mechanical properties, but also can improve the magnetism of the sintering bulk alloy.

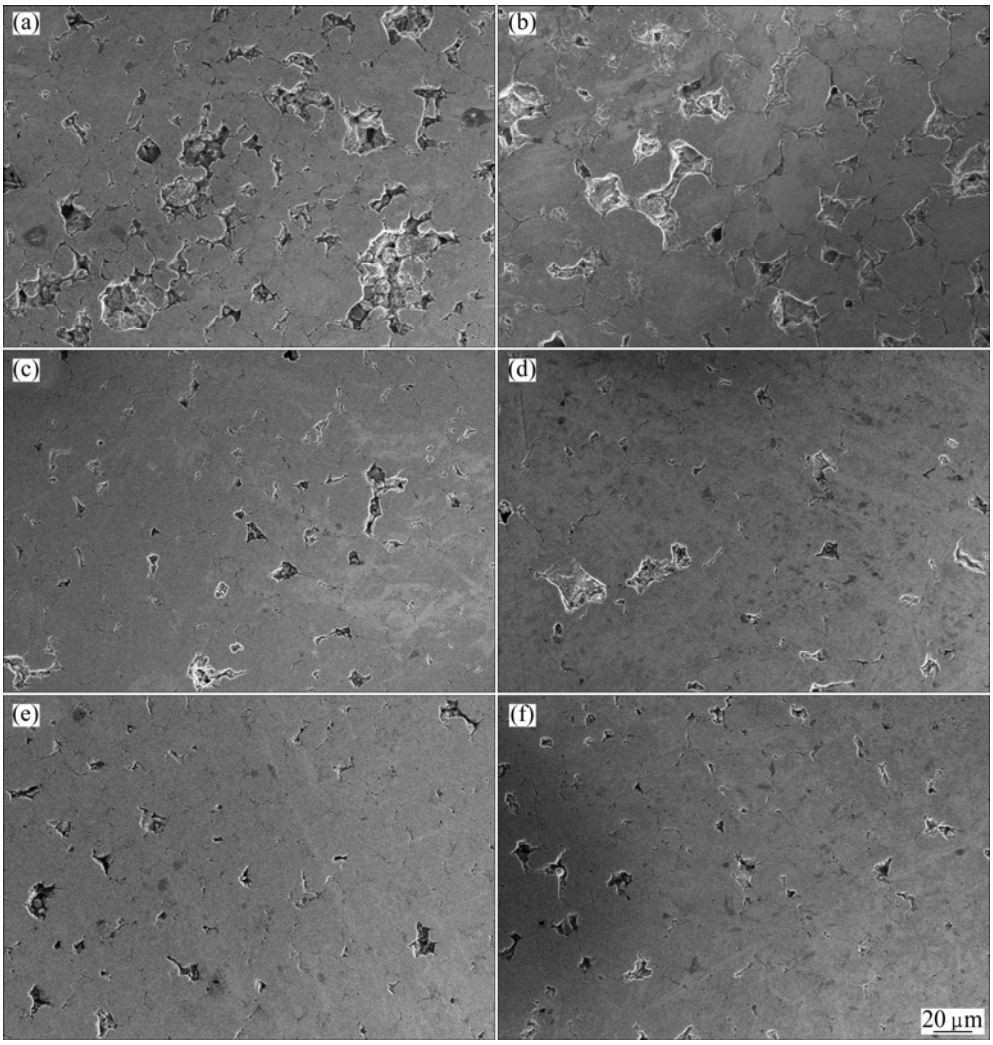

Fig. 7 SEM micrographs of $Fe_{75}Zr_3Si_{13}B_9$ bulk alloys sintered by SPS at different sintering temperatures: (a) 723.15 K; (b) 753.15 K; (c) 793.15 K; (d) 823.15 K; (e) 843.15 K; (f) 863.15 K

References

[1] ZHANG Jiu-xing, LIU Ke-gao, ZHOU Mei-ling. Development and application of spark plasma sintering [J]. Powder Metallurgy Technology, 2002, 20(3): 129−134. (in Chinese)

[2] NEAMTU B V, CHICINAS I, ISNARD O, CIASCAI I, CHIRIAC H, LOSTUN M. Magnetic properties of nanocrystalline Ni_3Fe compacts prepared by spark plasma sintering [J]. Intermetallics, 2013, 35: 98−103.

[3] ERIKSSON M, LIU Y, HU J F, GAO L, NYGREN M, SHEN Z J. Transparent hydroxyapatite ceramics with nanograin structure prepared by high pressure spark plasma sintering at the minimized sintering temperature [J]. Journal of the European Ceramic Society, 2011, 31(9): 1533−1540.

[4] MUNIR Z A, ANSELMI-TAMBURINI U, OHYANAGI M. The effect of electric field and pressure on the synthesis and consolidation of materials: A review of the spark plasma sintering method [J]. Journal of Materials Science Letters, 2006, 41(3): 763−777.

[5] XIAO Z Y, TANG C Y, ZHAO H D, ZHANG D T, LI Y Y. Effects of sintering temperature on microstructure and property evolution of $Fe_{81}Cu_2Nb_3Si_{14}$ soft magnetic materials fabricated from amorphous melt-apun ribbons by spark plasma sintering technique [J]. Journal of Non-Crystalline Solids, 2012, 358(1): 114−118.

[6] MUNIR Z A, QUACH D V, OHYANAGI M. Electric current activated of sintering: A review of the pulsed electric current sintering process [J]. Journal of the American Ceramic Society, 2011, 94(1): 1−19.

[7] WANG H C, LIU Y, PAN X H, FENG C D, AI F, ZHANG Y. Structure and magnetic properties of bulk $Fe_{56}Co_7Ni_7Zr_{10}B_{20}$ magnetic alloy fabricated by spark plasma sintering [J]. Journal of Alloys and Compounds, 2009, 477(1−2): 291−294.

[8] TEBER A, SCHOENSTEIN F, TETARD F, ABDELLAOUI M, JOUINI N. Effect of SPS process sintering on the microstructure and mechanical properties of nanocrystalline TiC for tools application [J]. International Journal of Refractory Metals and Hard Materials, 2012, 30(1): 64−70.

[9] YOSHIZAWA Y, OGUMA S, YAMAUCHI K. New Fe-based soft magnetic alloys composed of ultrafine grain structure [J]. Journal of Applied Physics, 1988, 64(10): 6044−6046.

[10] SUZUKI K, MAKINO A, INOUE A. Soft magnetic properties of nanocrystalline bcc Fe−Zr−B and Fe−M−B−Cu (M=transition metal) alloys with high saturation magnetization [J]. Journal of Applied Physics, 1991, 70(10): 6232−6235.

[11] WILLARD M A, LAUGHLIN D E，MCHENRY M E. Structure and magnetic properties of $(Fe_{0.5}Co_{0.5})_{88}Zr_7B_4Cu_1$ nanocrystalline alloys [J]. Journal of Applied Physics, 1998, 84(12): 6773−6777.

[12] TAKADATE K, KOJIMA A, MKINO A, INOUE A. Effect of Nd substitution on the soft magnetic properties of a nanocrystalline $Fe_{84}Nb_7B_9$ alloy [J]. Scripta Materialia, 2001, 44(8−9): 1401−1405.
[13] INOUE A, TAKEUCHI A. Recent development and application products of bulk glassy alloys [J]. Acta Materialia, 2011, 59(6): 2243−2267.
[14] HERZER G. Grain size dependence of coercivity and permeability in nanocrystalline ferromagnets [J]. IEEE Transactions on Magnetics, 1990, 26(5): 1397−1402.
[15] HERZER G. Grain structure and magnetism of nanocrystalline ferromagnets [J]. IEEE Transactions on Magnetics, 1989, 25(5): 3327−3329.
[16] HERZER G. Soft magnetic nanocrystalline materials [J]. Scripta Metallurgica et Materialia, 1995, 33(10−11): 1741−1756.

放电等离子烧结制备 $Fe_{75}Zr_3Si_{13}B_9$ 磁性材料

王兴华[1]，王 葛[1]，朱玉英[1]，鲍金峰[1]，杜雄飞[1]，李 强[1,2,3]

1. 燕山大学 国家冷轧板带装备及工艺工程技术研究中心，秦皇岛 066004;
2. 燕山大学 亚稳材料制备技术与科学国家重点实验室，秦皇岛 066004;
3. 河北工业大学 材料科学与工程学院，天津 300401

摘 要：采用机械合金化技术制备 $Fe_{75}Zr_3Si_{13}B_9$ 非晶合金粉体，利用 SPS 放电等离子烧结技术在不同烧结温度下将非晶合金粉体制备成 *d*20 mm×7 mm 的块体非晶纳米晶合金。采用 XRD 和 DSC 分析了 $Fe_{75}Zr_3Si_{13}B_9$ 非晶合金粉体的相组成、玻璃转变温度 T_g、开始晶化温度 T_x 和晶化峰温度 T_p。然后利用 XRD、SEM、Gleeble3500、VSM 分析不同烧结温度下块体的相转变、微观形貌、力学性能和磁性能。研究表明，在 500 MPa 的烧结压力下，随着烧结温度的升高，非晶相开始晶化形成非晶纳米晶双相结构，同时，样品的致密度、抗压强度、微观硬度、饱和磁化强度均显著提高。最后在 500 MPa 的烧结压力和 863.15 K 的烧结温度下，获得密度 6.9325 g/cm^3、抗压强度 1140.28 MPa、饱和磁化强度 1.28 T 的非晶纳米晶磁性材料。

关键词：机械合金化；非晶与纳米晶合金；饱和磁化强度；放电等离子烧结

(Edited by Hua YANG)